Supporting Information

High Performance Ambipolar Organic Field-Effect Transistors Based on Indigo Derivatives

Oratai Pitayatanakul, Toshiki Higashino, Tomofumi Kadoya, Masaki Tanaka, Hirotaka Kojima, Minoru Ashizawa, Tadashi Kawamoto, Hidetoshi Matsumoto, Ken Ishikawa and Takehiko Mori**

General: The data of Nuclear Magnetic Resonance spectrum (NMR), Infrared spectrum (IR) and Mass spectrum (MS) were obtained with a JEOL JNM-AL300 spectrometer, a Shimadzu Fourter Transform Infrared Spectrophotometer FTIR-8400S and a Shimadzu Mass Spectrometer, respectively. Wakogel® C-200 was used as a filler for column chromatography. For the sublimation process, the glass tubes were heated 24 h under a vacuum of 10^{-4} Pa at 330°C and 350°C for **1** and **2**, respectively.

Synthesis of 5,5'-dibromoindigo (1)

Following Scheme S1, **1** was prepared by iodination of **3**, followed by acetoxylation with silver acetate in acetic acid to afford 5-bromo-acetoxyindole (**5**), whose alkaline hydrolysis accompanied by air oxidation gave the corresponding **1**.

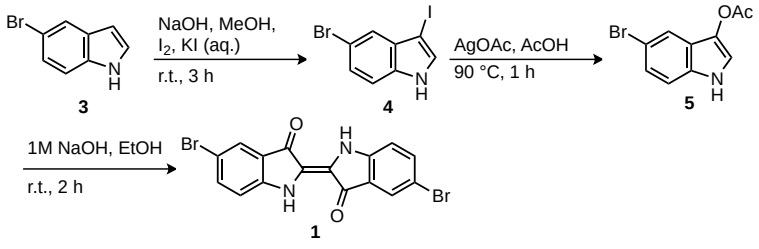

Scheme S1. Synthesis of **1**.

5-Bromo-3-iodoindole (4). To a solution of 5-bromoindole (**3**) (200 mg, 1.02 mmol) and sodium hydroxide (41 mg, 1.02 mmol) in methanol (10 ml) were added iodine

(259 mg, 1.02 mmol) and an aqueous solution (2 ml) of potassium iodide (169 mg, 1.02 mmol). After the mixture was stirred at room temperature for 3 h, water was added. The resulting precipitate was collected by filtration, washed with water, and dried to give 5-bromo-3-iodoindole (**4**) (315.8 mg, quant.) as a beige solid, which was used for the following reaction without purification because of its instability; EIMS *m/z*: 323 [M + 2], 321 [M^+]; ^{1}H NMR (300 MHz, $CDCl_3$, δ): 7.61 (s, 1H, Ar H), 7.31 (m, 2H, Ar H), 7.26 (s, 1H, Ar H).

3-Acetoxy-5-bromoindole (5). Silver acetate (327.6 mg, 1.96 mmol) was added to a solution of **4** (315.8 mg, 0.98 mmol) in acetic acid (8 ml). After stirring at 90°C for 1 h, the mixture was cooled to room temperature and filtrated. The filtrate was evaporated to dryness under reduced pressure. The residue was chromatographed on silica gel with dichloromethane (CH_2Cl_2) to give 3-acetoxy-5-bromoindole (**5**) (130 mg, 52% yield) as a dark blue solid; EIMS *m/z*: 255 [M + 2], 253 [M^+]; ^{1}H NMR (300 MHz, $CDCl_3$, δ): 7.89 (br, 1H, NH), 7.70 (s, 1H, Ar H), 7.38 (d, 1H, Ar H), 7.28 (m, 2H, Ar H), 2.36 (s, 3H, CH_3).

5,5'-Dibromoindigo (1). To a solution of **5** (560 mg, 2.2 mmol) in ethanol (50 ml) was added aqueous 1 M sodium hydroxide (40 ml). After the mixture was stirred at room temperature for 2 h, water was added. The resulting precipitate was collected by filtration, washed with water, and dried to give **1** (311 mg, 67% yield) as a dark blue solid. Compound **1** was purified by sublimation under 10^{-4} Pa at 330 °C for 24 h; EIMS *m/z*: 422 [M + 4], 420 [M + 2], 418 [M^+]; IR (KBr): ν = 3283 (NH), 1629 (C=O), 1607 (Ar), 1458, 1188, 1140, 1119, 1080 (Ar Br), 617 cm^{-1}.

Synthesis of 5,5'-diphenylindigo (2)

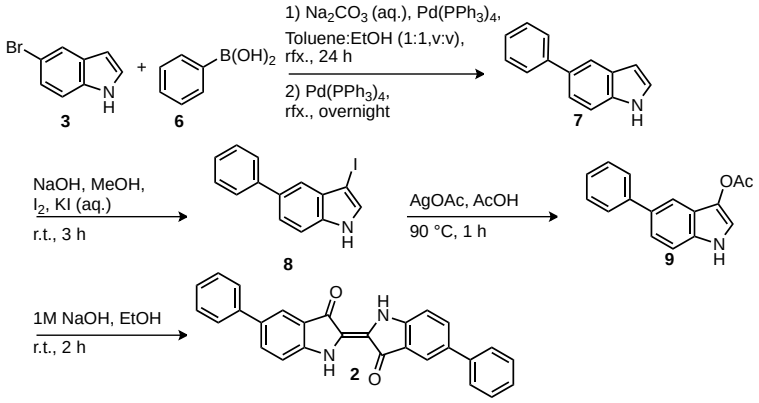

Scheme S2. Synthesis of **2**.

As shown in Scheme S2, Suzuki-Miyaura cross-coupling reaction was used to synthesize 5-phenylindole (**7**) in the first step, and similar methods to preparing **1** were applied to synthesize **2**.

5-Phenylindole (7). An aqueous solution of sodium carbonate (6 ml of a 1 M solution, 6 mmol) and tetrakis(triphenylphosphine)palladium(0) ($Pd(PPh_3)_4$) (51.3 mg, 0.044mmol) in 1:1 toluene-ethanol (6 ml) were added to a solution of **3** (500 mg, 2.55 mmol) and phenylboronic acid (**6**) (621.8 mg, 5.1 mmol) in 1:1 toluene-ethanol (6 ml), and the resulting mixture was heated at reflux under nitrogen for 24 h. $Pd(PPh_3)_4$ (51.3 mg, 0.044 mmol) in 1:1 toluene-ethanol (6 ml) was added, and reflux was continued under nitrogen overnight. After the mixture was cooled, the solvent was removed by evaporation and the resulting residue was purified by chromatography on silica gel with 9:1 hexane-ethyl acetate to give **7** (340 mg, 69% yield) as clear yellow oil; EIMS *m/z*: 193 [M^+].

5-Phenyl-3-iodoindole (8). To a solution of **7** (340 mg, 1.76 mmol) and sodium hydroxide (70.4 mg, 1.76 mmol) in methanol (18 ml) were added iodine (447 mg, 1.76 mmol) and an aqueous solution (3.5 ml) of potassium iodide (292.16 mg, 1.76 mmol). After the mixture was stirred at room temperature for 3 h, water was added.

The resulting precipitate was collected by filtration, washed with water, and dried to give 5-phenyl-3-iodoindole (**8**) (460 mg, 82% yield) as black oil, which was used for the following reaction without purification because of its instability; EIMS *m/z*: 319 [M^+].

3-Acetoxy-5-phenylindole (9). Silver acetate (480.7 mg, 2.88 mmol) was added to a solution of **8** (460 mg, 1.44 mmol) in acetic acid (12 ml). After stirring at 90°C for 1 h, the mixture was cooled to room temperature and filtrated. The filtrate was evaporated to dryness under reduced pressure. The residue was chromatographed on silica gel with chloroform ($CHCl_3$) to give 3-acetoxy-5-phenylindole (**9**) (184.5 mg, 51% yield) as a dark brown solid; EIMS *m/z*: 251 [M^+].

5,5'-Diphenylindigo (2). To a solution of **9** (469.8 mg, 1.87 mmol) in ethanol (55 ml) was added aqueous 1 M sodium hydroxide (110 ml). After the mixture was stirred at room temperature for 2 h, water was added. The resulting precipitate was collected by filtration, washed with water, and dried to give **2** (302.3 mg, 78% yield) as a dark purple solid. Compound **2** was purified by sublimation under 10^{-4} Pa at 350°C for 24 h; EIMS *m/z*: 414 [M^+]; IR (KBr): ν = 3376 (NH), 1622 (C=O), 1456, 1136, 1198, 758 (Ph), 590 cm^{-1}. Anal. calcd for $C_{28}H_{18}N_2O_2$: C 81.14, H 4.38, N 6.76; found: C 81.01, H 4.34, N 6.65.

Thermo Gravimetric-Different Thermal Analysis (TG-DTA)

In order to improve efficiency in the vacuum-deposition method, TG-DTA was measured to determine the decomposition temperature and thermal stability of the indigo derivatives. TG-DTA was measured by using Rigaku Themo Plus EVO II TG/DTA 8120/H. The measurements were carried out under N_2 atmosphere at 25°C-800°C at a heating rate of 10°C min^{-1}.

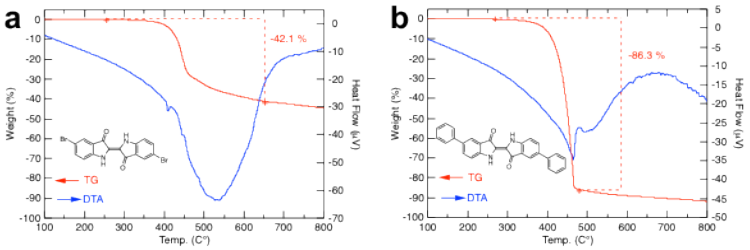

Figure S1. TG-DTA curves of a) **1** and b) **2** heated to 800 °C in N_2 atmosphere at a heating rate of 10°C min^{-1}.

DTA curves of **1** and **2** (Figure S1) show endothermic peaks starting at about 300°C, and clear endothermic peaks around 450°C and 540°C, respectively. The TG curves show that **1** loses 90% of its starting mass when it is heated up to 800°C, and the temperature of 5% mass loss is 390°C. Compound **2** affords higher thermal stability of 420°C with lower mass loss of 40% than **1** at 800°C. Compounds **1** and **2** exhibit no exothermic melting peaks because these molecules decompose before melting. In addition, **2** is expected to need a higher temperature than **1** to be evaporated due to the decomposition behavior and the thermal stability. This is reflected to the sublimation temperatures of **1** and **2**, 330 and 350°C, respectively.

Cyclic Voltammetry (CV) and Ultraviolet-Visible Spectroscopy (UV-Vis)

CV and UV-Vis was measured to determine the HOMO/LUMO levels and energy gaps of the indigo derivatives as shown in Figure S2 and S3. CV scan curves of **1** and **2** solutions were collected on Bi-Potentionstat ALS/DY2323 using Ag in 0.1 M $AgNO_3$ solution for a reference electrode, platinum (Pt) for a working electrode and carbon for a counter electrode in tetrabutylammonium hexafluorophosphate (Bu_4NPF_6) in a benzonitrile (C_6H_5CN) electrolyte solution at a scan rate of 100 mV s^{-1} at 150°C. HOMO and LUMO energy levels were estimated by assuming the

reference energy level of ferrocene/ferrocenium (Fc/Fc^+: $E^{1/2}$ = +0.31 V *vs.* $Ag/AgNO_3$ measured under identical conditions) to be 4.8 eV from the vacuum level.[36] UV-Vis spectra were collected on a Jasco Corporation V-560 UV/VIS Spectrophotometer in 1,1,2-trichloroethane ($CHCl_2CH_2Cl$) solutions and a Jasco Corporation V-630 UV/VIS Spectrophotometer for thin films.

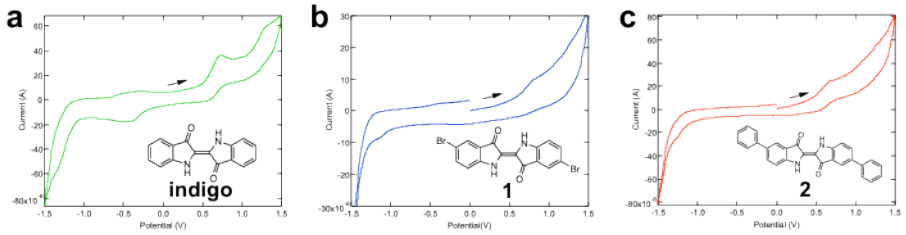

Figure S2. CV scan curves of a) indigo, b) **1**, and c) **2** in benzonitrile solutions *vs.* $Ag/AgNO_3$, which is 0.31 V *vs.* Fc/Fc^+.

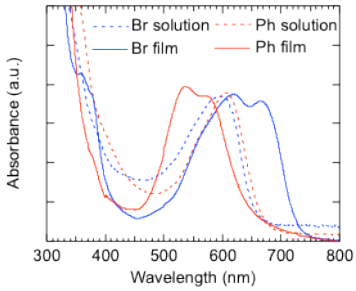

Figure S3. Optical absorption spectra of **1** (blue) and **2** (red).

Model of Ambipolar Transistors

Operation of ambipolar transistors has been investigated since the era of a-Si transistors,[S1,S2] but ordinary formulas do not consider the presence of unipolar saturated regions,[1,19,S3] which appear due to the difference between the electron (V_{TH}) and hole (V_{TH}') threshold voltages. We show here most general formulas of ambipolar transistors.

When V_{TH} = 0, characteristics of an n-channel unipolar transistor (Figure S4(a)) is obtained from the standard gradual channel operation.[S4]

$$I_D = \frac{W\mu_e}{L}\int_0^{V_{DS}} C(V_{GS} - V)\,dV = \frac{W\mu_e C}{L}\left(V_{GS}V_{DS} - \frac{1}{2}V_{DS}^2\right)$$

($V_{DS} < V_{GS}$) (S1)

Here the source-drain voltage, V_{DS}, and the source-gate voltage, V_{GS}, are both positive. This is the standard formula for the linear region ($V_{DS} < V_{GS}$). In the saturated region ($V_{DS} > V_{GS}$), the integration is limited to $0 < V < V_{GS}$ (Figure S4(b)), and the standard formula for the saturated region,

$$I_D = \frac{W\mu_e}{L}\int_0^{V_{GS}} C(V_{GS} - V)\,dV = \frac{W\mu_e C}{L}\left(V_{GS}^2 - \frac{1}{2}V_{GS}^2\right) = \frac{W\mu_e C}{2L}V_{GS}^2$$

($V_{GS} < V_{DS}$) (S2)

is obtained. In an ambipolar transistor, hole is injected from the drain, whose contribution is represented by the gradual channel approximation in $V_{GS} < V < V_{DS}$ (Figure S4(b)).

$$I_D = \frac{W\mu_h}{L}\int_{V_{GS}}^{V_{DS}} C(V - V_{GS})\,dV = \frac{W\mu_h C}{L}\left[\frac{V^2}{2} - V_{GS}V\right]_{V_{GS}}^{V_{DS}} = \frac{W\mu_h C}{2L}(V_{DS} - V_{GS})^2$$

(S3)

If the electron-hole recombination occurs immediately,[S5] the current in the ambipolar region is given by the sum of these two.

$$I_D = \frac{W\mu_e C}{2L}V_{GS}^2 + \frac{W\mu_h C}{2L}(V_{DS} - V_{GS})^2$$

($0 < V_{GS} < V_{DS}$) (S4)

This equation smoothly connects to Equation S1 at $V_{GS} = V_{DS}$. In an ambipolar transistor, we have to consider the reversed region, $V_{GS} < 0 < V_{DS}$ (Figure S4(c)),

where hole is the unique carrier. Since this is another linear region, the gradual channel approximation affords,

$$I_D = \frac{W\mu}{L}\int_0^{V_{DS}} C(|V_{GS}|+V)\,dV = \frac{W\mu_h C}{L}\left(\frac{1}{2}V_{DS}^2 - V_{GS}V_{DS}\right)$$

($V_{GS} < 0 < V_{DS}$) (S5)

where $V_{GS} < 0$ is used. This equation has an opposite sign to Equation S1, but in the output characteristics, this equation does not saturate at large V_{DS} because the coefficient of V_{DS}^2 is positive.

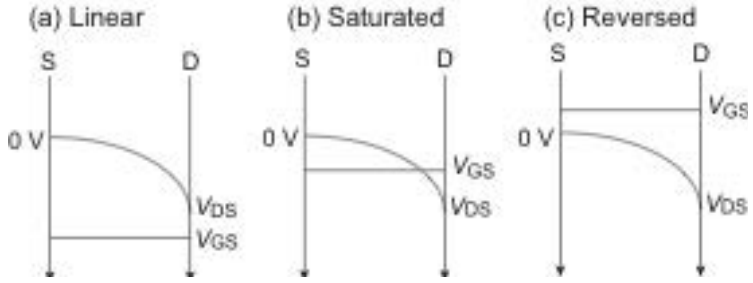

Figure S4. Potential distribution in an n-channel transistor.

A typical transfer characteristics derived from these equations are depicted in Figure S5. From large V_{GS} to small V_{GS}, the linear region ($V_{GS} > V_{DS}$) represented by Equation S1 is succeeded by the ambipolar region (Equation S4) at $V_{GS} = V_{DS}$, followed by the reversed region below $V_{GS} < 0$ (Equation S5). The characteristics in the ambipolar region ($0 < V_{GS} < V_{DS}$) follow V_{GS}^2, but other regions are basically V_{GS} linear (Equations S1 and S5). The current takes a minimum at $V_{GS} = V_{DS}/2$, but the minimum value is nonzero, because ambipolar transport occurs in this region. Actual ambipolar transistors exhibit a very sharp minimum or even an off region, and it is inappropriate to use these formulas to analyze actual ambipolar transistors. This is because hole transport does not start at $V_{GS} = V_{DS}$, if V_{TH}' is nonzero. In such a case, a

unipolar (electron transporting) saturated region appears just below $V_{GS} = V_{DS}$ (Figure 1).[2]

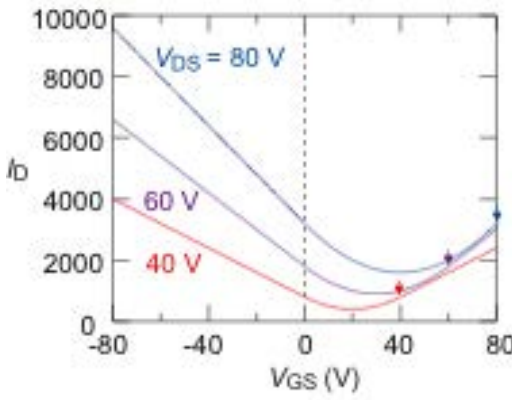

Figure S5. Transfer characteristics of an ambipolar transistor without unipolar saturated regions, where $W\mu_e C/L$ and $W\mu_e C/L$ are assumed to be 1.0.

When we consider V_{TH} and V_{TH}', we can divide the operation regions as shown in Figure 1, where the potential distribution is depicted in Figure S6. The characteristics are obtained replacing V_{GS} by $V_{GS} - V_{TH}$ in the above formulas, as represented by Equation 1 to 5.

The typical transfer characteristics are depicted in Figure S7. When V_{TH} = 10 V and V_{TH}' = –10 V are introduced, an off region appears for small V_{DS}, but the off region disappears above $V_{DS} > V_{TH} - V_{TH}'$ = 20 V. The ambipolar characteristics at large V_{DS} are similar to Figure S5.

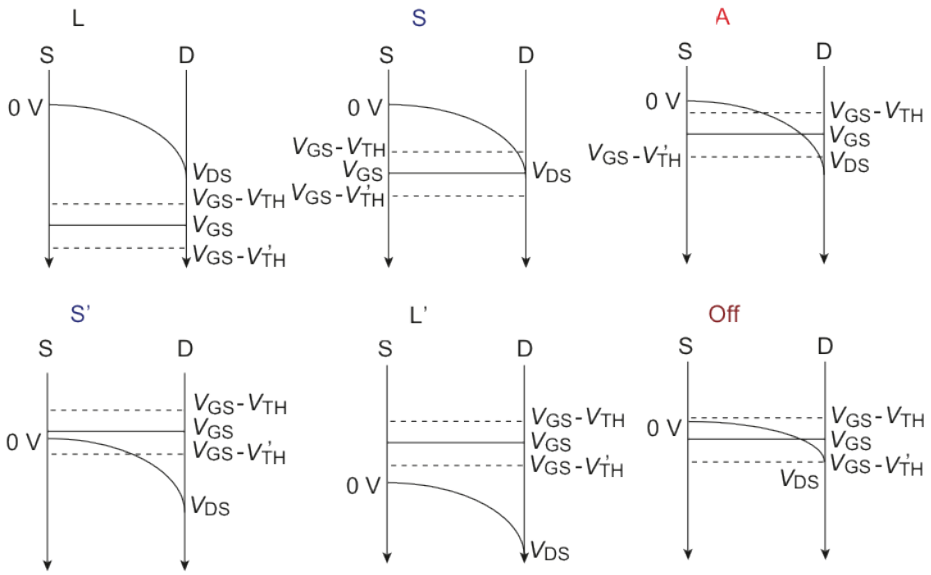

Figure S6. Potential distribution in an n-channel transistor.

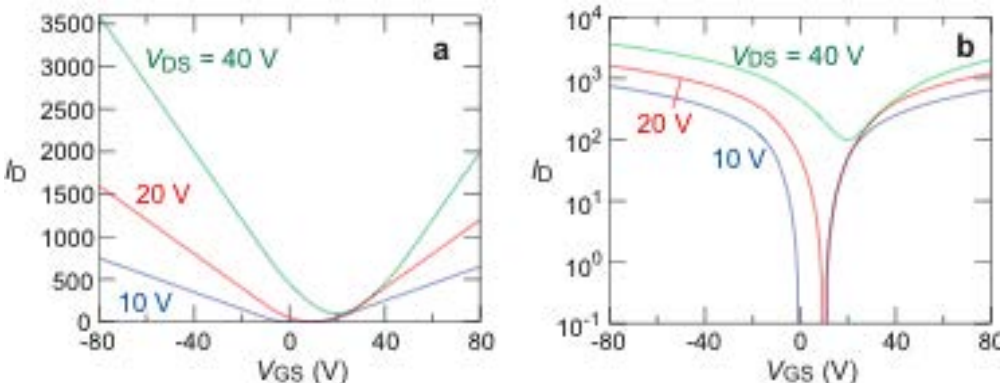

Figure S7. Transfer characteristics of an ambipolar transistor for V_{TH} = 10 V and V_{TH}' = –10 V, where $W\mu_eC/L$ and $W\mu_eC/L$ are assumed to be 1.0. a) A linear plot, and b) a log plot.

Crystal Structures

Crystals grown by the nitrogen flow method were used for the X-ray single crystal structure analyses (Table S1). The diffraction data of **1** were collected by a Rigaku four-circle diffractometer (AFC-7R) with graphite-monochromatized Mo-$K\alpha$ radiation (λ = 0.71069 Å). The X-ray oscillation photographs of **2** were taken

using a RIGAKU R-AXIS RAPID II imaging plate with Cu-$K\alpha$ radiation from a rotation anode source with a confocal multilayer X-ray mirror (RIGAKU VM-Spider, λ = 1.54187 Å). The structures of **1** and **2** were solved by the direct method (SIR2008) and refined by the full matrix least-squares procedure (SHELXL).[S6,S7] Anisotropic thermal parameters were adopted for all non-hydrogen atoms.

Table S1. Crystallographic data of **1** and **2**.

Compounds	**1**	**2**
Chemical formula	$C_{16}H_8N_2O_2Br_2$	$C_{28}H_{18}N_2O_2$
Crystal system	monoclinic	monoclinic
Formula weight	420.1	414.5
Shape	dark blue plate	dark violet plate
Space group	$P2_1/c$	$P2_1/c$
a [Å]	13.794(7)	21.2805(6)
b [Å]	4.462(3)	7.0108(2)
c [Å]	11.963(7)	6.5404(2)
β [°]	110.23(4)	92.739(2)
V [Å^3]	690.8(8)	974.67(5)
Z	2	2
T [K]	298	271
D_{calc} [g cm^{-3}]	2.020	1.412
Independent reflections	2015	1777
Observed reflections [$F^2 > 2.0\sigma(F^2)$]	1201	1020
$R1$ [$F^2 > 2.0\sigma(F^2)$]	0.045	0.069
$wR2$ [All reflections]	0.133	0.204
GOF	1.005	0.956
CCDC	1002555	1002556

Molecular Orbitals

HOMO and LUMO of Tyrian purple and **1** are calculated by Gaussian 09 package at B3LYP/6-31G(d,p) level as shown in Figure S8.[S8] HOMO and LUMO of **2** calculated by AM1 are shown in Figure S9.[S9] Geometry optimization based on both B3LYP/6-31G(d,p)[S8] and AM1[S9] indicates that phenyl planes are considerably tilted with respect to the central indigo plane, as observed in the actual crystal structure. The transfer integrals, t_i, listed in Figure 2 and 3 captions were estimated

from the intermolecular overlap integrals, S_i as $t_i = E \times S_i$ by assuming the energy level E to be –10 eV.[S10]

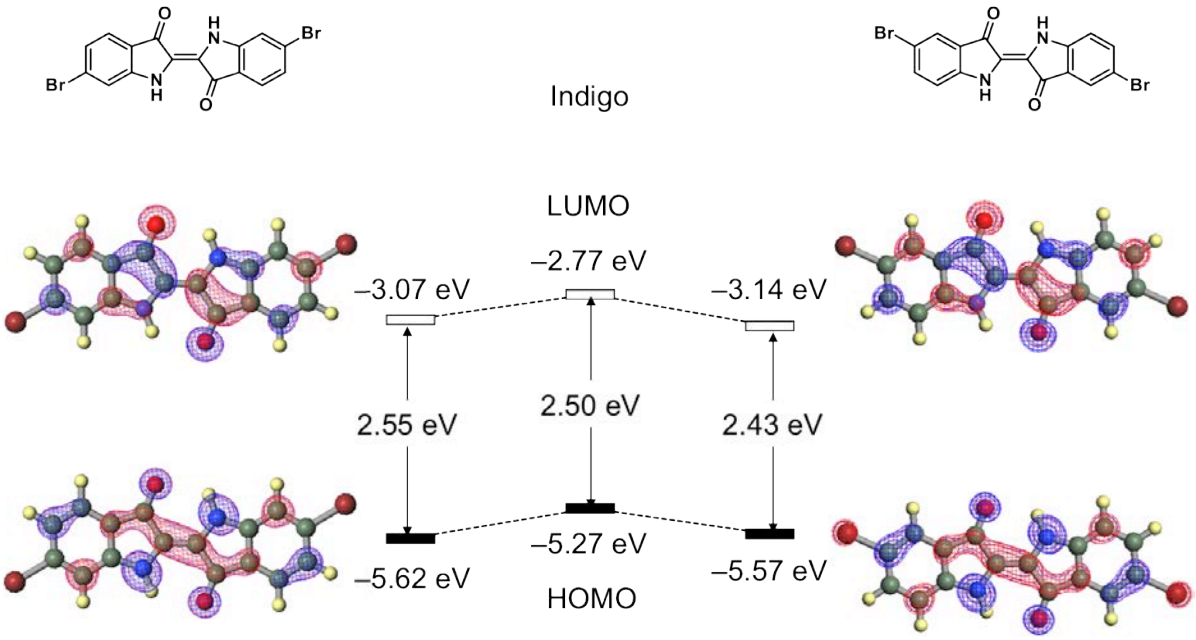

Figure S8. HOMO and LUMO of Tyrian purple and **1**.[43]

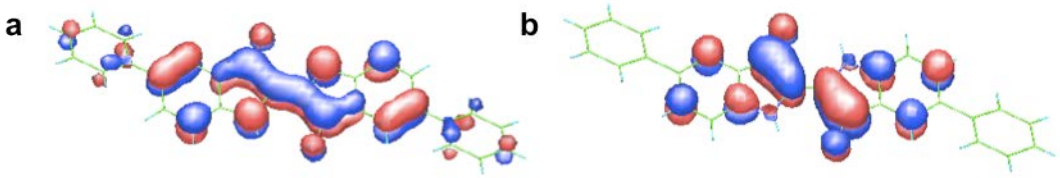

Figure S9. a) HOMO and b) LUMO of **2**.

Device Fabrication and Thin Film Properties

The transistors were prepared by using a commercially available heavily doped *n*-type Si wafer with 300 nm SiO_2 insulator (ε = 3.9 and the capacitance of 11.5 nF cm^{-2}) as a gate.[S11] A passivation layer of TTC was evaporated (ε = 2.5 and 20 nm thickness with the capacitance of 106 nF cm^{-2}),[11] and the resulting

overall capacitance of the gate dielectric was 10.4 nF cm^{-2}. Transistors on a PEN substrate were prepared by using PEDOT:PSS as a gate. A PEDOT:PSS film was spin-coated through a layer-by-layer process[S12] from a 5wt% DMSO solution containing 0.5wt% fluorosurfactant Zonyl. A Parylene C film was evaporated (ε = 3.1 and 900 nm thickness with the capacitance of 2.2 nF cm^{-2}),[S13] and the resulting overall capacitance of the gate dielectric was 3.6 nF cm^{-2}. Then the indigo derivatives (45 nm) were deposited at a rate of 0.1 Å s^{-1} under a pressure of 10^{-3} Pa. Gold source and drain electrodes were evaporated through a shadow mask (L/W = 100/1000 μm) at a pressure of 10^{-3} Pa to accomplish the bottom-gate top-contact transistors (Figure 1). The device was once taken out to the ambient atmosphere, and transferred into a vacuum prober system. Transistor characteristics were measured with a Keithley 4200 semiconductor parameter analyzer under vacuum. AFM images of thin films of **1** (45 nm), **2** (75 nm) on TTC (20 nm), and **2** (45 nm) on Parylene C (900 nm) were taken by an SII scanning probe microscope system SPI3800N and SPA-300 by using a Si_3N_4 cantilever. X-ray diffraction analyses of thin films of **1** (45 nm), **2** (75 nm) on TTC (20 nm)|SiO_2 substrates, and **2** (45 nm) on a Parylene C (900 nm)|PEN substrate were performed by X'pert-Pro-MRD using the θ - 2θ technique with Cu-$K\alpha$ radiation for $2° \leq 2\theta \leq 50°$.

Device Air Stability

Stability of indigo transistors after prolonged air exposure has been reported in Ref. [23]. We have found ambipolar operation of **1** even under ambient conditions (Figure S10), though the maximum mobilities are decreased to μ_h/μ_e = 0.027/0.01 $cm^2\,V^{-1}\,s^{-1}$ (μ_h/μ_e = 0.010/7.6×10^{-3} $cm^2\,V^{-1}\,s^{-1}$ for the average mobilities) after one week of air

exposure. Only hole transport has been observed in **2** with the maximum mobility of μ_h = 0.53 $cm^2 V^{-1} s^{-1}$ (μ_h = 0.28 $cm^2 V^{-1} s^{-1}$ for the average mobilities) under ambient conditions (Figure S11).

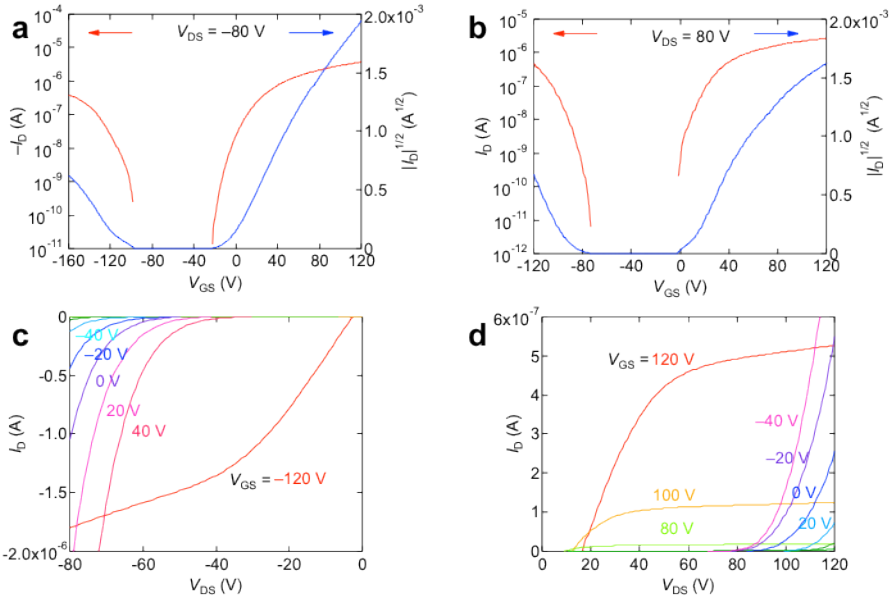

Figure S10. Transfer characteristics at a) V_{DS} = –80 V and b) V_{DS} = 80 V and output characteristics at c) V_{DS} < 0 and d) V_{DS} > 0 of thin-film transistors of **1** measured in air.

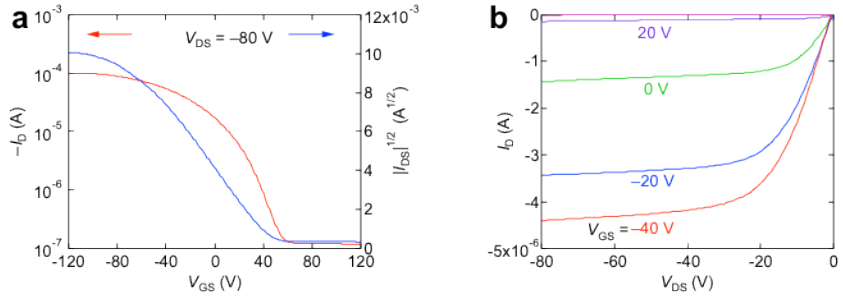

Figure S11. a) Transfer characteristics of thin-film transistors of **2** measured in air at V_{DS} = –80 V, and b) output characteristics for V_{DS} < 0.

References

[S1] H. Pfleiderer, *IEEE Trans. Electr. Dev.*, 1986, **33**, 145.

[S2] G. W. Neudeck, H. F. Bare, and K. Y. Chung, *IEEE Trans. Electr. Dev.*, 1987, **34**, 344.

[S3] R. Schmechel, M. Ahles, and H. von Seggern, *J. Appl. Phys*., 2005, **98**, 084511.

[S4] J. P. Colinge and C. A. Colinge, *Physics of Semiconductor Devices* (Springer, New York, 2002) p99-103.

[S5] G. Paasch, Th. Lindner, C. Rost-Bietsch, S. Karg, W. Ross, S. Scheinert, *J. Appl. Phys*., 2005, **98**, 084505.

[S6] M. C. Burla, R. Caliandro, M. Camalli, B. Carrozzini, G. L. Cascarano, L. D. Caro, C. Giacovazzo, G. Polidori, D. Siliqi, and R. Spagna, *J. Appl. Crystallogr*., 2007, **40**, 609.

[S7] G. M. Sheldrick, *Acta Crystallogr*. *Sect. A*, 2008, **64**, 112.

[S8] M. J. Frisch, G. W. Trucks, H. B. Schlegel, G. E. Scuseria, M. A. Robb, J. R. Cheeseman, G. Scalmani, V. Barone, B. Mennucci, G. A. Petersson, H. Nakatsuji,M. Caricato, X. Li,H.P. Hratchian, A. F. Izmaylov, J. Bloino, G. Zheng, J. L. Sonnenberg, M. Hada, M. Ehara, K. Toyota, R. Fukuda, J. Hasegawa, M. Ishida, T. Nakajima, Y. Honda, O. Kitao, H. Nakai, T. Vreven, J. A. Montgomery, Jr., J. E. Peralta, F. Ogliaro, M. Bearpark, J. J. Heyd, E. Brothers, K. N. Kudin, V. N. Staroverov, R. Kobayashi,J.Normand, K. Raghavachari, A. Rendell, J. C. Burant, S. S. Iyengar, J. Tomasi, M. Cossi, N. Rega, J. M. Millam, M. Klene, J. E. Knox, J. B. Cross, V. Bakken, C. Adamo, J. Jaramillo, R. Gomperts, R. E. Stratmann, O. Yazyev, A. J. Austin, R. Cammi,C. Pomelli, J. W. Ochterski, R. L. Martin, K. Morokuma, V. G. Zakrzewski, G. A. Voth, P. Salvador, J. J. Dannenberg, S. Dapprich, A. D. Daniels, O. Farkas, J. B. Foresman, J. V. Ortiz, J. Cioslowski, D. J. Fox, *Gaussian 09 (Revision B. 01)*, Gaussian, Inc., Wallingford CT, 2009.

[S9] M. J. S. Dewar, E. G. Zoebisch, E. F. Healy, and J. J. P. Stewart, *J. Am. Chem. Soc*., 1985, **107**, 3902.

[S10] T. Mori, A. Kobayashi, Y. Sasaki, H. Kobayashi, G. Saito, and H. Inokuchi, *Bull. Chem. Soc. Jpn*., 1984, **57**, 627.

[S11] K. J. Baeg, Y. Y. Noh, J. Ghim, B. Lim, and D.Y.Kim, *Adv. Funct. Mater*., 2008, **18**, 3678.

[S12] M. Vosgueritchian, D. J. Lipomi, and Z. Bao, *Adv. Funct. Mater.*, 2012, *22*, 421.

[S13] C. R. Newman, R. J. Chesterfield, M. J. Panzer, and C. D. Frisbie, *J. Appl. Phys.*, 2005, **98**, 084506.